

## High-temperature magnetic anomaly in the Kitaev hyperhoneycomb compound $\beta$ -Li<sub>2</sub>IrO<sub>3</sub>

Alejandro Ruiz,<sup>1,2</sup> Vikram Nagarajan,<sup>1,2</sup> Mayia Vranas,<sup>1,2</sup> Gilbert Lopez,<sup>1,2</sup> Gregory T. McCandless,<sup>3</sup> Itamar Kimchi,<sup>4</sup> Julia Y. Chan,<sup>5</sup> Nicholas P. Breznay,<sup>6</sup> Alex Frañó,<sup>7</sup> Benjamin A. Frandsen,<sup>8</sup> and James G. Analytis<sup>1,2</sup>

<sup>1</sup>*Department of Physics, University of California, Berkeley, California 94720, USA*

<sup>2</sup>*Materials Sciences Division, Lawrence Berkeley National Laboratory, Berkeley, California 94720, USA*

<sup>3</sup>*Department of Chemistry and Biochemistry, The University of Texas at Dallas, Richardson, Texas 75080, USA*

<sup>4</sup>*JILA, NIST and Department of Physics, University of Colorado, Boulder, Colorado 80309, USA*

<sup>5</sup>*Department of Chemistry, The University of Texas at Dallas, Richardson, Texas 75080, USA*

<sup>6</sup>*Department of Physics, Harvey Mudd College, Claremont, California 91711, USA*

<sup>7</sup>*Department of Physics, University of California, San Diego, California 92093, USA*

<sup>8</sup>*Department of Physics and Astronomy, Brigham Young University, Provo, Utah 84602, USA*



(Received 28 May 2019; revised manuscript received 8 November 2019; accepted 9 January 2020; published 12 February 2020)

We report the existence of a high-temperature magnetic anomaly in the three-dimensional Kitaev candidate material,  $\beta$ -Li<sub>2</sub>IrO<sub>3</sub>. Signatures of the anomaly appear in magnetization, heat capacity, and muon spin relaxation measurements. The onset coincides with a reordering of the principal axes of magnetization, which is thought to be connected to the onset of Kitaev-like correlations in the system. The anomaly also shows magnetic hysteresis with a spatially anisotropic magnitude that follows the spin-anisotropic exchange anisotropy of the underlying Kitaev Hamiltonian. We discuss possible scenarios for a bulk and impurity origin.

DOI: [10.1103/PhysRevB.101.075112](https://doi.org/10.1103/PhysRevB.101.075112)

### I. INTRODUCTION

Since Khaliullin and Jackeli [1,2] first pointed out that Kitaev's frustrated compass model [3] on a honeycomb lattice could be realized in  $4d$  and  $5d$  transition metal systems with octahedral coordination, such materials have become one of the most promising routes to experimentally realizing a quantum spin liquid. The ground state itself, first described by Kitaev [3], is characterized by the long range order of flux degrees of freedom, emerging from the fractionalization of the local spins into Majorana excitations. The ideal Kitaev model couples orthogonal directions of spin along the three different bond directions,

$$\mathcal{H} = K \sum_{\langle ij \rangle} S_i^\gamma S_j^\gamma, \quad (1)$$

where  $\gamma = x, y, z$  specify the three compass directions of the Kitaev exchange,  $K$ . Importantly, in the  $\beta$ -Li<sub>2</sub>IrO<sub>3</sub> and  $\gamma$ -Li<sub>2</sub>IrO<sub>3</sub> materials, one of these Kitaev axes is exactly parallel to the crystallographic  $b$  axis.

Although some low-temperature signatures of novel excitations have been reported [4], the magnetic order present in all candidate materials dominate most of their properties (zigzag order in the case of  $\alpha$ -RuCl<sub>3</sub> and  $\alpha$ -Na<sub>2</sub>IrO<sub>3</sub>, and incommensurate order in  $\alpha$ ,  $\beta$ ,  $\gamma$ -Li<sub>2</sub>IrO<sub>3</sub> species) [5–10]. However, many recent studies have found high-temperature signatures of these exotic states or proximity thereto. For example, recent spectroscopic and thermodynamic studies of  $\alpha$ -RuCl<sub>3</sub> [11–17] have reported evidence for the onset of nearest-neighbor Kitaev correlations, consistent with a proposal by Motome and coauthors of a thermal crossover from a paramagnet to a spin-“fractionalized” state [18–20]. Similar studies have

extended these conclusions to  $\alpha$ ,  $\beta$ ,  $\gamma$ -Li<sub>2</sub>IrO<sub>3</sub> and  $\alpha$ -Na<sub>2</sub>IrO<sub>3</sub> systems [21–23]. In the case of the  $\beta$ - and  $\gamma$ -Li<sub>2</sub>IrO<sub>3</sub> systems this temperature range is also associated with strong deviations from Curie-Weiss susceptibility, and a dramatic reordering of the principal axes of magnetization [24].

The nature of the ground state at these elevated temperatures is therefore of considerable interest [18–23]. However, due to the small size of the samples, relatively few studies have explored the three-dimensional  $\beta$ -Li<sub>2</sub>IrO<sub>3</sub> materials in this temperature range. In this work, we focus on the magnetic and thermal properties of  $\beta$ -Li<sub>2</sub>IrO<sub>3</sub>, and reveal the presence of a weak magnetic anomaly at  $\sim 100$  K. The transition is associated with the ferromagneticlike ordering of a small moment, whose anisotropy closely follows the Kitaev principal axes. We discuss various scenarios of bulk and impurity origin.

### II. EXPERIMENTAL RESULTS

Single crystals of  $\beta$ -Li<sub>2</sub>IrO<sub>3</sub> were synthesized using standard techniques described in the Supplemental Material [25] (SM, Sec. S1). The three-dimensional nature of  $\beta$ -Li<sub>2</sub>IrO<sub>3</sub> is realized in the hyperhoneycomb arrangement of the Ir atoms shown in Fig. 1(a), while the low-field anisotropic magnetic susceptibility is shown in Fig. 1(b). In Fig. 1(c), we contrast the inverse  $b$ -axis susceptibility measured at 1 T and 0.1 T to show that, above 100 K, the magnetization is truly field independent with an effective spin  $\mathcal{J} = 1/2$ , which can be completely understood as paramagnetic spins coupled to their orbital environment (see SM, Sec. S2A for details). Below  $T_f = 38$  K, the system orders into an incommensurate state with noncoplanar and counter-rotating spins [8,9]. At  $\sim 100$  K

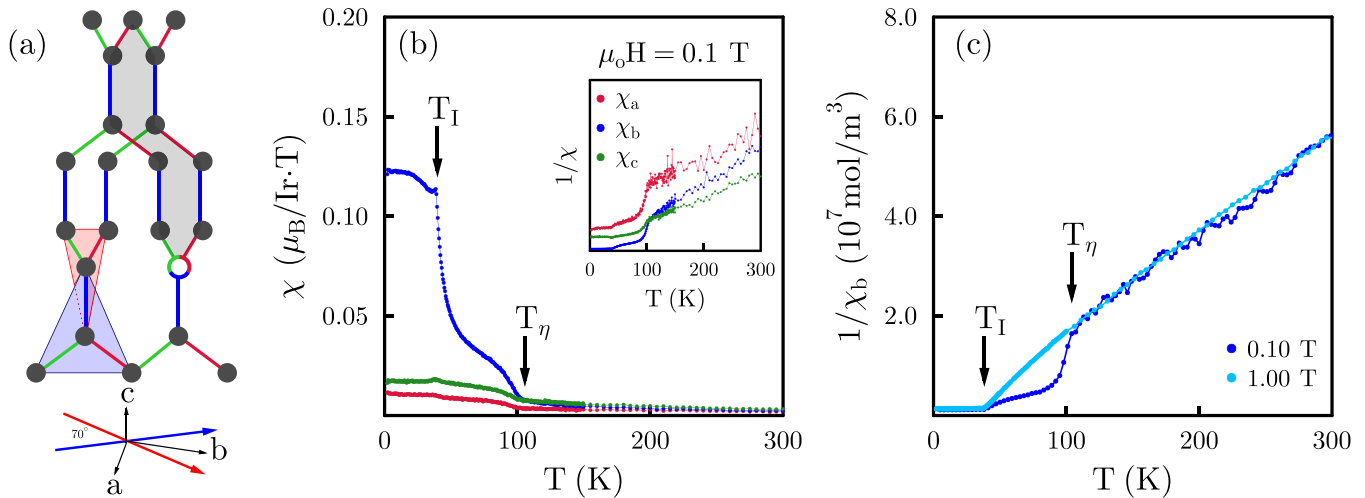


FIG. 1. (a) Three-dimensional structure of  $\beta$ - $\text{Li}_2\text{IrO}_3$ , where the red, green, and blue colors correspond to orthogonal compass directions of the Kitaev model. The two triangles, situated  $70^\circ$  apart, show the possible environments for a magnetic ion in  $\beta$ - $\text{Li}_2\text{IrO}_3$ , and determine the  $g$ -factor anisotropy. Also shown is a site vacancy which can trap flux excitations in a Kitaev spin liquid, creating a large local moment. (b) The anisotropic magnetic susceptibility of  $\beta$ - $\text{Li}_2\text{IrO}_3$  for an applied magnetic field of 0.1 T. At  $T_I = 38$  K, the system transitions into an incommensurate spiral state with noncoplanar, counter-rotating moments. When a small magnetic field is applied ( $H < 0.5$  T), a magnetic anomaly is also observed at 100 K. Inset shows inverse susceptibility, clearly showing a reordering of the principal axes of susceptibility at  $\sim 100$  K. (c) Comparison of the inverse  $\hat{b}$ -axis susceptibility for 1.0 T and 0.1 T. The low-field data shows two distinct behaviors: a linear response above 100 K and a strong deviation from Curie-Weiss behavior  $100 > T > 40$  K.

the principal axes of the magnetization reorder due to the presence of strong Kitaev-like correlations [24] [Fig. 1(b), inset], such that the  $b$  axis becomes dominant. Our data shows that this reordering occurs due to the presence of a magnetic anomaly at  $T_\eta$ , which can only be observed using low applied magnetic fields. The smearing of this transition at higher fields [Fig. 1(c)] is likely why it has remained hidden in previous measurements (see SM, Sec. S2-S3) [24,26–28]. As the field decreases, this transition becomes apparent, as seen in the comparison data shown in Fig. 1(c). The magnetic signal is extremely reproducible between different samples and batches (see also Supplemental Material [25], SM Fig. 6), and independent of the synthesis environment (crucible material or source of starting elements), and sample volume (see SM, Sec. S5). In addition, we find no evidence of competing crystalline phases in single crystal x-ray diffraction measurements (see SM, Sec. S1 for details). Similar results were also observed in  $\gamma$ - $\text{Li}_2\text{IrO}_3$ , as described in SM, Sec. S2. This suggests an impurity phase is extremely unlikely as an origin of this magnetic anomaly. Notably, the transition temperature is conspicuously close to the temperature window under intense study in the 2D Kitaev candidate systems, where there is thought to be evidence of emergent, fractional excitations [21–23].

Figures 2(a)–2(c) show the field-dependent magnetization below  $T_\eta$  along three crystallographic directions, illustrating clear hysteresis behavior, and a coercive field that increases with decreasing temperature [in our case we parametrize this with the anisotropy field  $H_a$ , whose temperature dependence is shown in Fig. 3(d)]. The insets in Fig. 2 show the hysteresis curve after a linear background was subtracted, determined from the high field susceptibility in Fig. 1(c).

The spatial dependence of the anisotropy field  $H_a$  is independent of crystallographic direction, which is very surprising given the anisotropic nature of the crystal structure and

magnetism. In contrast, the (background subtracted) saturation moment  $M_s$  appears to vary by a factor of  $\sim 10$ , mirroring the anisotropy of the susceptibility, which is thought to originate from the presence of Kitaev correlations [24,29]. We note that, while this background subtraction makes the precise determination of the saturation moment difficult, the hysteresis loops in any direction rise with approximately the same gradient, suggesting they approach saturation with the same functional form. Therefore, independent of the background subtraction, this implies  $M_s$  must be strongly spatially anisotropic. In typical magnetically ordered systems, or even in spin glasses, the behavior is usually the other way around, where the saturation moment is isotropic (since it is related to the local moment), while the coercive field is anisotropic (since it is related to the anisotropy of the free energy and/or structural anisotropies of domain boundaries) [30]. The spatial anisotropy of  $M_s$  suggests a strong orbital component to the magnetic species that freezes/orders at  $T_\eta$ .

Figure 3 shows the angular dependence of the magnetic torque of  $\beta$ - $\text{Li}_2\text{IrO}_3$  at fixed fields and temperatures, respectively. Figure 3(a) displays the onset of hysteretic behavior in the  $ab$  plane upon cooling below 100 K when sweeping angle from  $0^\circ$  to  $180^\circ$  and back. Upon lowering temperature further, hysteresis occurs in a wider angular range, corresponding to the larger anisotropy field and the larger angle needed to allow for a greater component of  $H$  along  $b$ . Hysteresis is observed for  $H$  aligned in both the  $bc$  and  $ab$  planes, as seen in Figs. 3(b) and 3(c). With increasing field, the angular range of hysteresis decreases until eventually it disappears.

The anisotropy field  $H_a$ , where the moment associated with the magnetic anomaly saturates, is shown by the blue dots in the phase diagram of Fig. 3(d) (see SM Sec. S4 for low-temperature determination of  $H_a$ ).  $H_a$  appears to be indifferent to the phase boundary as the system crosses

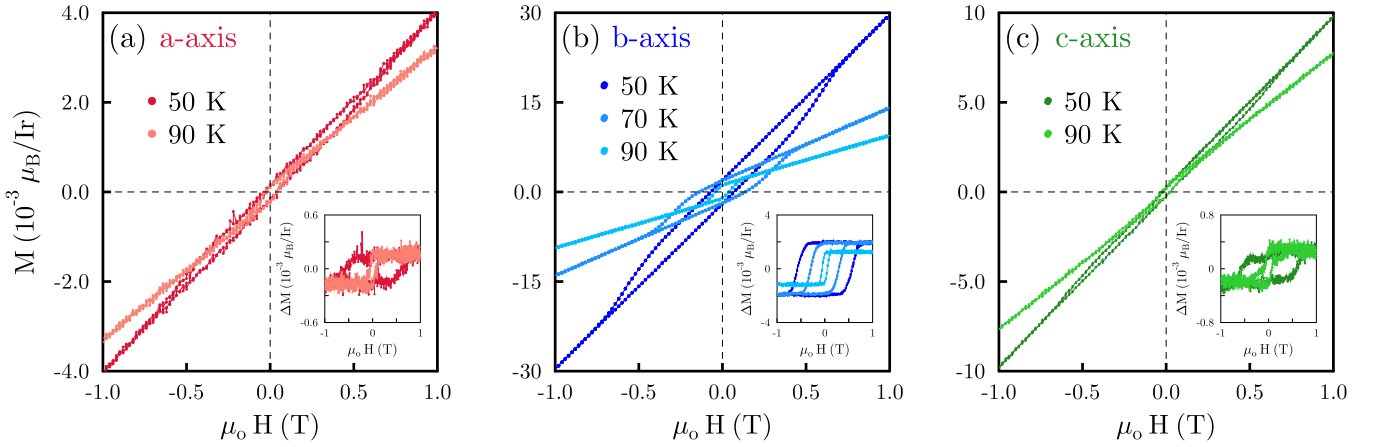


FIG. 2. (a)–(c) Hysteresis behavior was observed in  $\beta$ - $\text{Li}_2\text{IrO}_3$  below  $T_\eta = 100$  K. The figure insets show the data after the linear background corresponding to the high-field susceptibility is subtracted to indicate the isotropy of the anisotropic field  $H_a$  along the three principal axes.

into the incommensurate phase marked by  $H^*$ . On the other hand,  $H_a$  terminates at the zero temperature at  $H_a(0) \sim H^*(0)$  within experimental error, suggesting the incommensurate and magnetic anomaly might share a common energy scale [Fig. 4(d)]; the field required to polarize the high-temperature magnetic anomaly is the same as that required to flip the incommensurate phase into the field induced zigzag phase (FIZZ).

In Fig. 4(a), we show the zero-field-cooled (ZFC) and field-cooled (FC) magnetization curves using 0.1 T (inset), and their difference (main figure). The latter shows the natural form expected of a magnetic order parameter growing below  $T_\eta$ . Figure 4(b) shows the relaxation (DC) heat capacity

measurements on powder of  $\beta$ - $\text{Li}_2\text{IrO}_3$  as well as on powder of a nonmagnetic analog.  $\beta$ - $\text{Li}_2\text{PtO}_3$  was synthesized by a similar procedure as stated above for  $\beta$ - $\text{Li}_2\text{IrO}_3$  but with starting reagents Pt and  $\text{Li}_2\text{CO}_3$  [31]. The inset in Fig. 4(b) shows that no clear phase transition is observed in the region of interest around  $T_\eta$ . However,  $C_p/T$  vs  $T$  clearly shows that the total heat capacity of these two materials starts to differ below  $\sim T_\eta$ . Above 100 K, where the signal is dominated by phonons, the heat capacity of  $\beta$ - $\text{Li}_2\text{IrO}_3$  and  $\beta$ - $\text{Li}_2\text{PtO}_3$  are nearly indistinguishable. Therefore, the magnetic contribution can be isolated by subtracting the nonmagnetic background from  $\beta$ - $\text{Li}_2\text{PtO}_3$ . Figure 4(c) shows that the magnetic entropy ( $dS_m = C_p/T dT$ ) reaches  $\sim 1/4 R \ln 2$  at  $T_\eta$ . This is

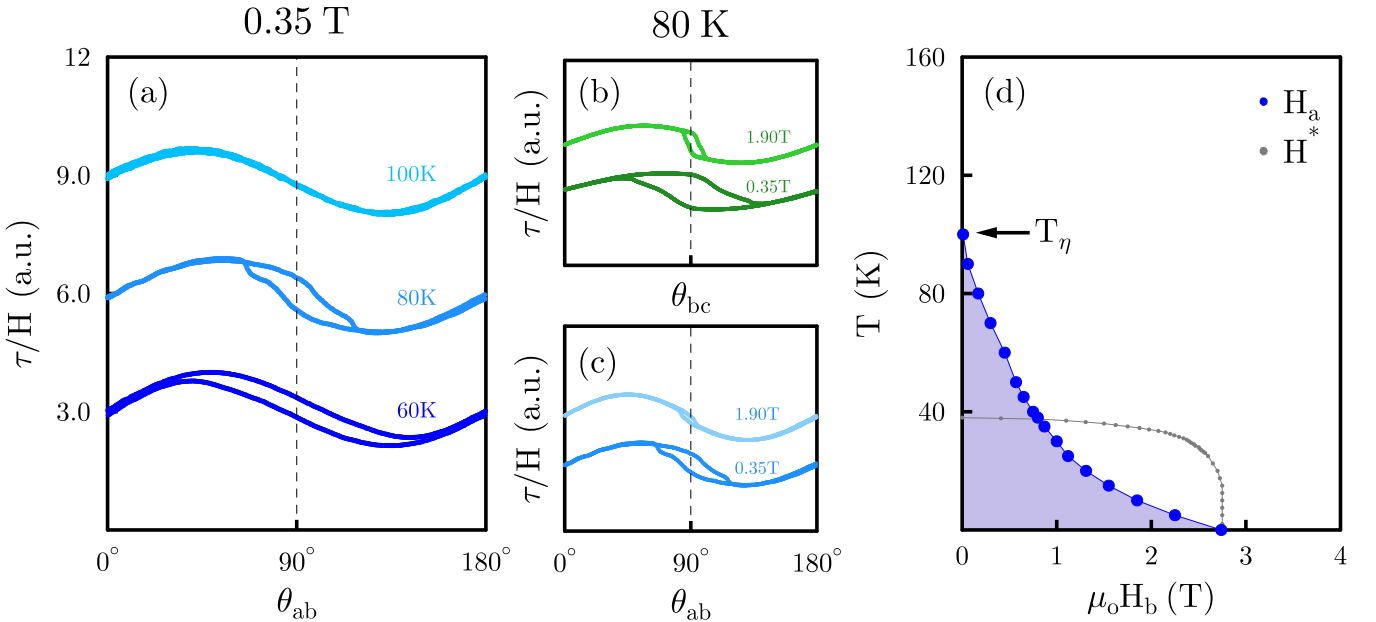


FIG. 3. (a) Angular dependent torque,  $\tau_a = 1/2(\chi_b - \chi_c)H^2 \sin 2\theta_{ab}$ , also shows hysteretic behavior below  $T_\eta$  for an applied field  $H = 0.35$  T. (b),(c) Hysteresis is observed for rotations in the  $ab$  and  $bc$  planes, but not in the  $ac$  plane. This behavior disappears at high fields, as it is evident in the data presented for 80 K. In this case  $\theta = 0$  corresponds to  $H \parallel b$  for rotations in the  $bc$  and  $ab$  planes. (d) The anisotropy field  $H_a$  was extracted from  $M(H)$  and  $\tau/H(\theta)$  measurements.  $H_a$  appears to be indifferent to the low temperature phase boundary, and it terminates  $H_a(0) \sim H^*(0)$ , suggesting the incommensurate and magnetic anomaly might share a common energy scale (see SM, Sec. S4 for low temperature determination).

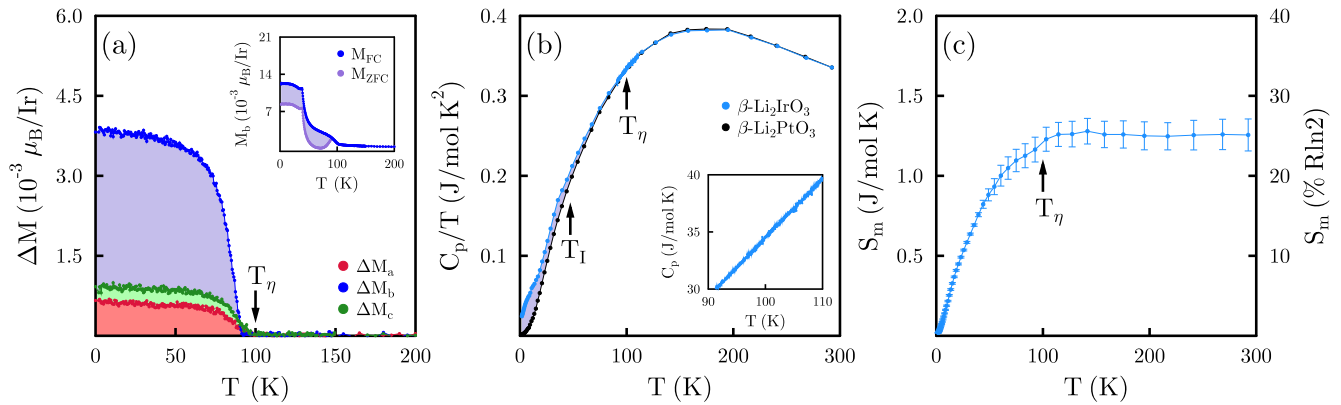


FIG. 4. (a) Inset shows the field-cooled (FC) and zero-field-cooled (ZFC) magnetization with a 0.1 T field applied along the  $b$  axis, while the main panel shows the magnetic irreversibility  $\Delta M = M_{FC} - M_{ZFC}$  for all three axes. (b) dc heat capacity was measured on a powder sample of  $\beta\text{-Li}_2\text{IrO}_3$  (blue points). The figure inset shows the area of attention from 90 to 110 K. No sharp transition was detected. A nonmagnetic isostructure,  $\beta\text{-Li}_2\text{PtO}_3$ , was also measured to isolate the magnetic contribution to the heat capacity (black points). The two curves start to deviate below 100 K. Moreover,  $\beta\text{-Li}_2\text{IrO}_3$  has a nonzero intercept at low temperature,  $\gamma = 0.02 \text{ J/mol K}^2$ . (c) The magnetic entropy was calculated by taking the difference between the two data sets in (b), and integrating over temperature,  $dS = C_p/T dT$ . At  $T_\eta$ , the magnetic entropy reaches  $\sim 1/4 R \ln 2$ .

in broad agreement with the results presented in Ref. [21] for  $\alpha\text{-Li}_2\text{IrO}_3$  (although the paper cites the value  $1/2 R \ln 2$ , close examination of the vertical axes shows that it is actually closer to  $1/4\text{--}1/3$ ). A maximum in  $C/T$  is also observed around 140 K, which is at odds with the findings in Ref. [21] but agrees with the most recent data in Ref. [28]. The weak magnetic anomaly at  $T_\eta$  freezes a very small fraction of the degrees of freedom, consistent with the smallness of the frozen/ordered moment itself.

Muon spin relaxation ( $\mu\text{SR}$ ) measurements were performed on the same powder sample as the above heat capacity (crystallographic information on SM, Sec. S1). Our measurements confirm that this feature in the magnetization and heat capacity data is intrinsic to  $\beta\text{-Li}_2\text{IrO}_3$ . As seen in Fig. 5(a), our  $\mu\text{SR}$  results show a clear increase in the zero-field (ZF) relaxation rate at 100 K, precisely the same temperature at which the magnetization and heat capacity features were observed. A model-independent comparison of the asymmetry spectra reveals that the change in relaxation begins at 100 K and grows like an order parameter [Fig. 5(b)], which is confirmed by fitting a model and extracting the temperature-dependent relaxation rate [Fig. 5(c)]. Further details are given in the SM, Sec. S6 and Refs. [32–34] therein. The relaxation can be fully decoupled with a very modest longitudinal field of 50 G, indicating the development of weak, static magnetism in  $\beta\text{-Li}_2\text{IrO}_3$  below 100 K. We note that this type of magnetism is completely different from the long-range magnetically ordered state below  $\sim 38$  K in this system, which manifests in the  $\mu\text{SR}$  data as rapid oscillations and damping in the early-time portion of the asymmetry spectra [35–37]. The  $\mu\text{SR}$  results are consistent with magnetization and heat capacity data which show the presence of a magnetic anomaly at  $T_\eta$ .

The  $\mu\text{SR}$  data suggests an impurity origin of the magnetic anomaly (like the presence of intergrowths) is unlikely, since all or nearly all of the muons experience a change below  $T_\eta$ . However, dynamics associated with Li disorder could also be a possible origin for the anomaly at  $T_\eta$ . In principle, the line shape of the asymmetry data, which is strongly Gaussian, can

be used to distinguish this possibility. In some systems, such disorder has been shown to lead to exponential line shapes [38], though other materials have associated Gaussian shapes with such Li dynamics [38–40]. As pointed out by a helpful referee, our data cannot rule out Li dynamics as a possible source of the magnetic anomaly. However, it is difficult to understand why this anomaly would coincide in temperature with the reordering of the principal axes of magnetization of the Ir lattice [Fig. 1(b)], nor why it would be affected by Ru substitution, as described below [Fig. 5(d)]. In addition, ordering of dilute magnetic impurities (which can lead to ferromagnetic transitions in magnetic semiconductors) can be excluded since these lead to dramatic changes in the asymmetry data below the transition temperature, whereas we see a relatively small increase in the muon relaxation rate below  $T_\eta$  [see Fig. 5(a)] [41–43]. Finally, the high reproducibility of the amplitude of the transition in the magnetization would argue against these extrinsic scenarios (see Supplemental Material [25], Fig. 6).

The role of disorder is nevertheless a very interesting one, and to investigate this a little further, we introduce disorder via ruthenium substitution. Ru-doped  $\text{Li}_2\text{IrO}_3$  was synthesized in two stages. First, a powder of  $\text{Li}_2\text{RuO}_3$  was synthesized by mixing powders of  $\text{Li}_2\text{CO}_3$  and Ru with excess  $\text{Li}_2\text{CO}_3$  (1.05:1). The powder was ground and pressed into a pellet and placed into an alumina crucible. The pellet heated in air for 84 h at  $1010^\circ\text{C}$  with slow cooling time. After, the  $\text{Li}_2\text{RuO}_3$  powder was ground with stoichiometric ratios for desired ruthenium content, again with excess lithium. The powder was again ground and pelletized, and heated in air for 24 h at  $1050^\circ\text{C}$  with slow cooling time. Single crystals were extracted from the powder. In Fig. 5(d) we illustrate the field-cooled and zero-field-cooled magnetization curves for various amounts of Ru substituted materials. It is immediately clear that the incommensurate transition at  $T_I$  is suppressed, broadening into a broad crossover. This broadening leads to a hump in the magnetization, which grows systematically with Ru substitution. Such features are common in disordered

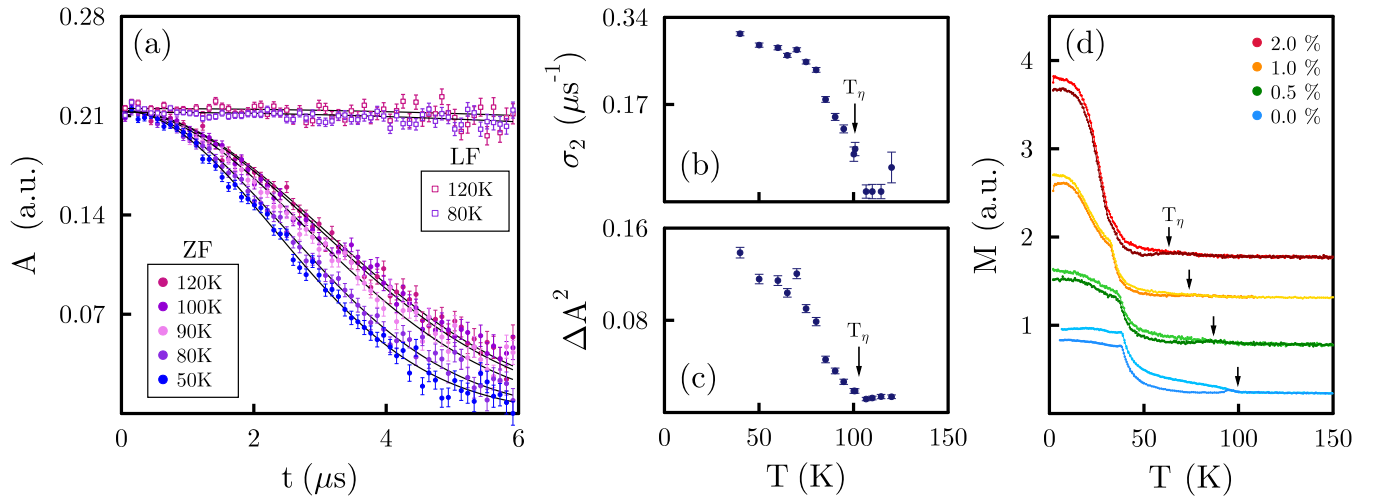


FIG. 5. (a)  $\mu\text{SR}$  asymmetry,  $A(t)$ , spectra at selected temperatures measured in zero field (ZF) and a 50 G longitudinal field (LF). The ZF relaxation rate shows a clear increase below  $T_\eta$ . This relaxation can be decoupled with a very modest LF, indicating the development of weak, static magnetism. Solid lines are Gaussian fits to the data. (b) The asymmetry  $A(t) = a_0 e^{-t^2(\sigma_1^2 + \sigma_2^2)/2}$  has two contributions: a  $T$ -independent nuclear contribution  $\sigma_1$  and a  $T$ -dependent electronic contribution  $\sigma_2$ . The  $T$ -dependent  $\sigma_2$  evolves like an order parameter below  $T_\eta$ . (c) A model independent metric,  $\Delta A^2(T) = \sum_i \frac{(A_i^{150\text{K}} - A_i^T)^2}{(A_i^{150\text{K}})^2}$ , confirms the results of the fits in panel (b). (d) Ruthenium substituted samples show a clear effect of disorder: just as the incommensurate transition is suppressed, so too is the transition at 100 K, which is observed by the difference of zero-field-cooled (ZFC) and field-cooled (FC) magnetization curves taken with 0.01 T. Note that substitution amounts are given in nominal values. Actual values are significantly lower, below the resolution of our EDX measurements. Nevertheless, the systematics show clear trends.

magnets and often indicate the formation of a spin glass at low temperature [44,45]. The magnetic anomaly at 100 K is similarly suppressed, indicating that it is strongest in our cleanest materials. In addition, since Ru likely goes on the Ir site, the observed suppression may suggest the moment arises from the Ir sublattice.

### III. DISCUSSION

The thermodynamic and spectroscopic evidence unambiguously establishes the existence of a high-temperature magnetic anomaly in  $\beta\text{-Li}_2\text{IrO}_3$ ; there exists a sharp signature in the magnetic susceptibility and a crossover in the heat capacity, while the  $\mu\text{SR}$  data shows that the magnetic moment is static and exists throughout the volume of the sample. Below the incommensurate phase which onsets at  $T_I = 38$  K, the signatures of the magnetic anomaly persist. Strikingly, the anisotropy field  $H_a$  penetrates the incommensurate phase boundary in both field and temperature with complete impunity, suggesting they are independent [see Fig. 3(c)].

The existence of competing phases is widely known in these materials. In  $\beta\text{-Li}_2\text{IrO}_3$ , for example, it is known that a zigzag phase is close in energy and can be induced with the application of relatively small fields [27,46,47]. However, the  $\mu\text{SR}$  data unambiguously rules this out, as the presence of such a phase would lead to oscillations in the muon relaxation. Another possibility is a valence-bond transition, similar to that seen under pressure in  $\alpha\text{-RuCl}_3$  [48] or  $\beta\text{-Li}_2\text{IrO}_3$  [49–52]. However, the spin dimerization has an associated structural distortion that leads to strong hysteresis on warming and cooling, and this is absent in the current data. The  $\mu\text{SR}$  data is more consistent with a disordered magnet, like a spin glass. To

explain our data, the moment of the disordered species would have to be extremely weak as, according to our fits, the local field is of the order of a few gauss (by contrast the local field in  $\text{Na}_2\text{IrO}_3$  is an order of magnitude larger [35]). Even supposing that the true moment is somehow screened from the muons (which itself would require an exotic explanation given the absence of itinerant electrons to Kondo screen), the smallness of the induced moment in our magnetic measurements would suggest a highly dilute magnetic species. This, however, is difficult to reconcile with the high transition temperature, the sample-to-sample reproducibility, and the heat capacity anomaly, all of which are rare in typical examples of dilute spin glasses [53]. Moreover, the absence of relaxation effects, magnetic and thermal memory effects, and exchange bias is inconsistent with a spin glass scenario. On the other hand, as discussed above, Li dynamics could onset at higher temperatures and lead to a magnetic signature and, although it is unclear why this would onset at exactly the same temperature where the principal axes of magnetization reorder, nor why it has the same anisotropy, we cannot rule out this possibility.

Moreover, the basic characteristics of the magnetic anomaly at  $T_\eta$  are inconsistent with a dilute magnetic semiconductor scenario, in which magnetic defects order ferromagnetically. The onset at 100 K is much higher than the known ordering at  $T_I = 38$  K. In particular,  $\beta\text{-Li}_2\text{IrO}_3$  is a Mott insulator with a local moment on every Ir site, as evident from  $1/T$  Curie-Weiss dependence and from the well studied spiral magnetic order, unlike a semiconductor. This is a crucial difference; magnetic dopant ions can be present here, and they can magnetize the local moment, but it seems highly unlikely that they give a ferromagnetic signature at temperatures much higher than the intrinsic large-moment magnetic order  $T_I$ .

Nevertheless, there are other clues in the properties of this high-temperature phase that point to its origins. The saturation moment  $M_s$ , for example, is strongly anisotropic (Fig. 2). This conclusion can be seen to be independent of the background subtraction, since if  $M_s$  was isotropic the hysteresis loops along each crystallographic direction would not be the same shape. Moreover, the isotropy of the hysteresis, parametrized by the field  $H_a(i)$  ( $i \in a, b, c$ ), illustrates that the hysteresis does not come from domain formation (which would be influenced by the orthorhombic structure), but from the anisotropy in the free energy itself. This can be seen by the following argument. In uniaxial ferromagnets, the anisotropy field is given by the ratio of the anisotropic free energy  $K_a$  and the saturation moment  $M_s$ , so that the observation of an isotropic  $H_a(i) \sim K_a(i)/M_s(i)$  suggests  $M_s(i)$  follows the free energy anisotropy. From this we can make two conclusions. First, the smallness of the  $M_s$  and its spatial anisotropy strongly suggest an orbital origin. Secondly, this anisotropy exactly follows the magnetic principal axes and not the structural anisotropy of the orthorhombic crystal. Notably  $M_s$  picks out the Kitaev  $b$  axis as the dominant direction, just like the incommensurate phase. The magnetic species at  $T_\eta$  inherits signatures of Kitaev spin-spin correlations in the anisotropy of its energy landscape, but at the same time ordering a moment with a strongly orbital character, not of the local magnetic (Ir) ions.

Reconciling the dual character of this magnetic anomaly will require extensive future studies, but we speculate as to some possible scenarios here. For example, recent theoretical studies of Jahn-Teller distortions in related systems have shown the possible emergence of spin-nematic degrees of freedom. These could give rise to an emergent magnetic species that orders at relatively high temperatures [54], and couple together spin and orbital interactions, leading to nematic order with possibly the signatures we observe. However, we have performed structural refinements above and below  $T_\eta$  and found no significant changes in the positions of any atomic species, suggesting weak Jahn-Teller effects (see SM S1). Another possibility is the scalar chiral spin order recently suggested as an explanation for the sawtooth torque anomaly observed in  $\text{RuCl}_3$  and  $\gamma\text{-Li}_2\text{IrO}_3$  [55]. We note that the anomalous torque onsets at exactly 100 K, and extends into the incommensurate state. However, other studies have suggested that such anomalies can be understood by a field-dependent response with an anisotropic  $g$  factor [56]. The association of a phase transition with the onset of the torque anomaly, reported here, should assist in distinguishing these scenarios.

Finally, we comment on an interesting possibility that might be a middle ground between these different scenarios. Recent theoretical studies of site dilution in Kitaev spin liquids have revealed that vacancies form an emergent magnetic species [57,58] [Fig. 1(a)]. In this picture, the local fractionalization of spin degrees of freedom form moments in three-dimensional systems that interact via the spin liquid [57]. This may look like a disordered phase in a muon experiment, since there is no long range order of a local moment. However, such a phase could show a true thermal phase transition as

the spin degrees of freedom fractionalize to form the medium through which these moments interact [18]. We note that Raman spectroscopy in  $\beta\text{-Li}_2\text{IrO}_3$  has reported the presence of fermionic excitations at finite energy (presumably arising from spin fractionalization), but not of a phase transition [22]. On the other hand, evidence for such fractionalization in this temperature range has been reported in  $\alpha\text{-RuCl}_3$  and  $\alpha\text{-Li}_2\text{IrO}_3$  [11–17,59]. The fact that this appears as a crossover in the  $\alpha$ -type structures and a phase transition in  $\beta$ ,  $\gamma$ -type structures may simply reflect the different dimensionality of the materials.

#### IV. CONCLUSION

In  $\beta, \gamma\text{-Li}_2\text{IrO}_3$ , it is known that the magnetic principle axes reorder at  $\sim 100$  K [24,27,28]. At high temperatures, the magnetism follows the structural anisotropy, whereas at low temperature, it is determined by the spin-spin correlations, likely of the Kitaev type [29,60] (see also an extended discussion in SM, Sec. S2). Here we have shown that this reordering is actually accompanied by a bulk, intrinsic phase transition that is only visible at low fields ( $H < 0.5$  T), perhaps explaining why it has been overseen in previous measurements of this compound. The identity of this phase is unlikely to be one of the nearby ordered states known in the phase diagram of these systems, nor do its properties appear consistent with disordered phases like a typical spin glass. Rather, the observation of an anisotropic saturation moment that follows the Kitaev principal axes could arise if the ordered moment had an orbital origin that is tied to the spin-spin correlations of the Kitaev system. In this sense, the order at  $T_\eta$  involves the ordering of a spin-orbital magnetic species. Given the intrinsic nature of the magnetic anomaly, we expect similar subtle states to appear in related materials, which should be observable given sufficiently careful experiments in this temperature range.

#### ACKNOWLEDGMENTS

The authors would like to thank Anthony Carrington, Chandra Varma, Natalia Perkins, Roser Valenti, and Philip Gegenwart for fruitful discussions. In addition, material synthesis and experimental measurements were supported by the Department of Energy Early Career Award, Office of Basic Energy Sciences, Materials Sciences and Engineering Division, under Contract No. DE-AC02-05CH11231. A.R. also acknowledges support from the National Science Foundation Graduate Research Fellowship under Grant No. DGE 1106400. V.N. acknowledges support from the National Science Foundation Graduate Research Fellowship Grant No. DGE 1752814. M.V. acknowledges support from the UC LEADS program. N.P.B. was supported by the Gordon and Betty Moore Foundations EPiQS Initiative through Grant No. GBMF4374. J.Y.C. acknowledges Grant No. NSF-DMR-1700030. I.K. was supported by a National Research Council Fellowship through the National Institute of Standards and Technology.

- [1] G. Jackeli and G. Khaliullin, *Phys. Rev. Lett.* **102**, 017205 (2009).
- [2] J. Chaloupka, G. Jackeli, and G. Khaliullin, *Phys. Rev. Lett.* **105**, 027204 (2010).
- [3] A. Kitaev, *Ann. Phys. (NY)* **321**, 2 (2006).
- [4] Y. Kasahara, T. Ohnishi, Y. Mizukami, O. Tanaka, S. Ma, K. Sugii, N. Kurita, H. Tanaka, J. Nasu, Y. Motome, T. Shibauchi, and Y. Matsuda, *Nature (London)* **559**, 227 (2018).
- [5] Y. Singh and P. Gegenwart, *Phys. Rev. B* **82**, 064412 (2010).
- [6] X. Liu, T. Berlijn, W.-G. Yin, W. Ku, A. Tsvelik, Y.-J. Kim, H. Gretarsson, Y. Singh, P. Gegenwart, and J. P. Hill, *Phys. Rev. B* **83**, 220403(R) (2011).
- [7] R. D. Johnson, S. C. Williams, A. A. Haghighirad, J. Singleton, V. Zapf, P. Manuel, I. I. Mazin, Y. Li, H. O. Jeschke, R. Valentí, and R. Coldea, *Phys. Rev. B* **92**, 235119 (2015).
- [8] A. Biffin, R. D. Johnson, I. Kimchi, R. Morris, A. Bombardi, J. G. Analytis, A. Vishwanath, and R. Coldea, *Phys. Rev. Lett.* **113**, 197201 (2014).
- [9] A. Biffin, R. D. Johnson, S. Choi, F. Freund, S. Manni, A. Bombardi, P. Manuel, P. Gegenwart, and R. Coldea, *Phys. Rev. B* **90**, 205116 (2014).
- [10] S. C. Williams, R. D. Johnson, F. Freund, S. Choi, A. Jesche, I. Kimchi, S. Manni, A. Bombardi, P. Manuel, P. Gegenwart, and R. Coldea, *Phys. Rev. B* **93**, 195158 (2016).
- [11] L. J. Sandilands, Y. Tian, K. W. Plumb, Y.-J. Kim, and K. S. Burch, *Phys. Rev. Lett.* **114**, 147201 (2015).
- [12] A. Banerjee, C. A. Bridges, J.-Q. Yan, A. A. Aczel, L. Li, M. B. Stone, G. E. Granroth, M. D. Lumsden, Y. Yiu, J. Knolle, S. Bhattacharjee, D. L. Kovrizhin, R. Moessner, D. A. Tennant, D. G. Mandrus, and S. E. Nagler, *Nat. Mat.* **15**, 733 (2016).
- [13] A. Banerjee, J. Yan, J. Knolle, C. A. Bridges, M. B. Stone, M. D. Lumsden, D. G. Mandrus, D. A. Tennant, R. Moessner, and S. E. Nagler, *Science* **356**, 1055 (2017).
- [14] S.-H. Do, S.-Y. Park, J. Yoshitake, J. Nasu, Y. Motome, Y. S. Kwon, D. T. Adroja, D. J. Voneshen, K. Kim, T.-H. Jang, J.-H. Park, K.-Y. Choi, and S. Ji, *Nat. Phys.* **13**, 1079 (2017).
- [15] A. Banerjee, P. Lampen-Kelley, J. Knolle, C. Balz, A. A. Aczel, B. Winn, Y. Liu, D. Pajerowski, J. Yan, C. A. Bridges, A. T. Savici, B. C. Chakoumakos, M. D. Lumsden, D. A. Tennant, R. Moessner, D. G. Mandrus, and S. E. Nagler, *npj Quantum Mater.* **3**, 8 (2018).
- [16] Y. Kasahara, K. Sugii, T. Ohnishi, M. Shimozawa, M. Yamashita, N. Kurita, H. Tanaka, J. Nasu, Y. Motome, T. Shibauchi, and Y. Matsuda, *Phys. Rev. Lett.* **120**, 217205 (2018).
- [17] Y. Wang, G. B. Osterhoudt, Y. Tian, P. Lampen-Kelley, A. Banerjee, T. Goldstein, J. Yan, J. Knolle, H. Ji, R. J. Cava, J. Nasu, Y. Motome, S. E. Nagler, D. Mandrus, and K. S. Burch, *arXiv:1809.07782*.
- [18] J. Nasu, M. Udagawa, and Y. Motome, *Phys. Rev. Lett.* **113**, 197205 (2014).
- [19] J. Nasu, M. Udagawa, and Y. Motome, *Phys. Rev. B* **92**, 115122 (2015).
- [20] J. Nasu, J. Knolle, D. L. Kovrizhin, Y. Motome, and R. Moessner, *Nat. Phys.* **12**, 912 (2016).
- [21] K. Mehawat, A. Thamizhavel, and Y. Singh, *Phys. Rev. B* **95**, 144406 (2017).
- [22] A. Glamazda, P. Lemmens, S.-H. Do, Y. S. Choi, and K.-Y. Choi, *Nat. Commun.* **7**, 12286 (2016).
- [23] A. Revelli, M. M. Sala, G. Monaco, C. Hickey, P. Becker, F. Freund, A. Jesche, P. Gegenwart, T. Eschmann, F. L. Buessen, S. Trebst, P. H. M. van Loosdrecht, J. v. d. Brink, and M. Grüninger, *arXiv:1905.13590*.
- [24] K. A. Modic, T. E. Smidt, I. Kimchi, N. P. Breznay, A. Biffin, S. Choi, R. D. Johnson, R. Coldea, P. Watkins-Curry, G. T. McCandless, J. Y. Chan, F. Gandara, Z. Islam, A. Vishwanath, A. Shekhter, R. D. McDonald, and J. G. Analytis, *Nat. Commun.* **5**, 4203 (2014).
- [25] See Supplemental Material at <http://link.aps.org/supplemental/10.1103/PhysRevB.101.075112> for information regarding the crystal synthesis and structural characterization, as well as further details on magnetization, torque, heat capacity, and muon spin relation measurements.
- [26] T. Takayama, A. Kato, R. Dinnebier, J. Nuss, H. Kono, L. S. I. Veiga, G. Fabbri, D. Haskel, and H. Takagi, *Phys. Rev. Lett.* **114**, 077202 (2015).
- [27] A. Ruiz, A. Frano, N. P. Breznay, I. Kimchi, T. Helm, I. Oswald, J. Y. Chan, R. J. Birgeneau, Z. Islam, and J. G. Analytis, *Nat. Commun.* **8**, 961 (2017).
- [28] M. Majumder, F. Freund, T. Dey, M. Prinz-Zwick, N. Büttgen, Y. Skourski, A. Jesche, A. A. Tsirlin, and P. Gegenwart, *Phys. Rev. Mater.* **3**, 074408 (2019).
- [29] I. Kimchi, R. Coldea, and A. Vishwanath, *Phys. Rev. B* **91**, 245134 (2015).
- [30] S. Blundell, *Magnetism in Condensed Matter* (Oxford University Press, Oxford, 2001).
- [31] F. Freund, S. C. Williams, R. D. Johnson, R. Coldea, P. Gegenwart, and A. Jesche, *Sci. Rep.* **6**, 35362 (2016).
- [32] Y. Uemura, in *Muon Science: Muons in Physics, Chemistry and Materials*, edited by S. Lee, R. Cywinski, and S. Kilcoyne (Taylor & Francis, New York, 1999).
- [33] S. J. Blundell, *Contemp. Phys.* **40**, 175 (2010).
- [34] A. Yaouanc and P. D. de Réotier, *Muon Spin Rotation, Relaxation, and Resonance: Applications to Condensed Matter*, 1st ed. (Oxford University Press, Oxford, 2011).
- [35] S. K. Choi, R. Coldea, A. N. Kolmogorov, T. Lancaster, I. I. Mazin, S. J. Blundell, P. G. Radaelli, Y. Singh, P. Gegenwart, K. R. Choi, S.-W. Cheong, P. J. Baker, C. Stock, and J. Taylor, *Phys. Rev. Lett.* **108**, 127204 (2012).
- [36] M. Majumder, R. S. Manna, G. Simutis, J. C. Orain, T. Dey, F. Freund, A. Jesche, R. Khasanov, P. K. Biswas, E. Bykova, N. Dubrovinskaia, L. S. Dubrovinsky, R. Yadav, L. Hozoi, S. Nishimoto, A. A. Tsirlin, and P. Gegenwart, *Phys. Rev. Lett.* **120**, 237202 (2018).
- [37] S. Choi, S. Manni, J. Singleton, C. V. Topping, T. Lancaster, S. J. Blundell, D. T. Adroja, V. Zapf, P. Gegenwart, and R. Coldea, *Phys. Rev. B* **99**, 054426 (2019).
- [38] T. E. Ashton, J. V. Laveda, D. A. MacLaren, P. J. Baker, A. Porch, M. O. Jones, and S. A. Corr, *J. Mater. Chem. A* **2**, 6238 (2014).
- [39] J. Sugiyama, H. Nozaki, M. Harada, K. Kamazawa, Y. Ikedo, Y. Miyake, O. Ofer, M. Månsson, E. J. Ansaldo, K. H. Chow, G. Kobayashi, and R. Kanno, *Phys. Rev. B* **85**, 054111 (2012).
- [40] P. J. Baker, I. Franke, F. L. Pratt, T. Lancaster, D. Prabhakaran, W. Hayes, and S. J. Blundell, *Phys. Rev. B* **84**, 174403 (2011).
- [41] S. R. Dunsiger, J. P. Carlo, T. Goko, G. Nieuwenhuys, T. Prokscha, A. Suter, E. Morenzoni, D. Chiba, Y. Nishitani, T.

- Tanikawa, F. Matsukura, H. Ohno, J. Ohe, S. Maekawa, and Y. J. Uemura, *Nat. Mater.* **9**, 299 (2010).
- [42] Z. Deng, C. Jin, Q. Liu, X. Wang, J. Zhu, S. Feng, L. Chen, R. Yu, C. Arguello, T. Goko, F. Ning, J. Zhang, Y. Wang, A. Aczel, T. Munsie, T. Williams, G. Luke, T. Kakeshita, S. Uchida, W. Higemoto, T. Ito, B. Gu, S. Maekawa, G. Morris, and Y. Uemura, *Nat. Commun.* **2**, 422 (2011).
- [43] K. Zhao, Z. Deng, X. C. Wang, W. Han, J. L. Zhu, X. Li, Q. Q. Liu, R. C. Yu, T. Goko, B. Frandsen, L. Liu, F. Ning, Y. J. Uemura, H. Dabkowska, G. M. Luke, H. Luetkens, E. Morenzoni, S. R. Dunsiger, A. Senyshyn, P. Böni, and C. Q. Jin, *Nat. Commun.* **4**, 1442 (2013).
- [44] K. Mehawat, G. Sharma, and Y. Singh, *Phys. Rev. B* **92**, 134412 (2015).
- [45] S. Manni, Y. Tokiwa, and P. Gegenwart, *Phys. Rev. B* **89**, 241102(R) (2014).
- [46] I. Rousochatzakis and N. B. Perkins, *Phys. Rev. B* **97**, 174423 (2018).
- [47] S. Ducatman, I. Rousochatzakis, and N. B. Perkins, *Phys. Rev. B* **97**, 125125 (2018).
- [48] G. Bastien, G. Garbarino, R. Yadav, F. J. Martinez-Casado, R. Beltrán Rodríguez, Q. Stahl, M. Kusch, S. P. Limandri, R. Ray, P. Lampen-Kelley, D. G. Mandrus, S. E. Nagler, M. Roslova, A. Isaeva, T. Doert, L. Hozoi, A. U. B. Wolter, B. Büchner, J. Geck, and J. van den Brink, *Phys. Rev. B* **97**, 241108(R) (2018).
- [49] N. P. Breznay, A. Ruiz, A. Frano, W. Bi, R. J. Birgeneau, D. Haskel, and J. G. Analytis, *Phys. Rev. B* **96**, 020402(R) (2017).
- [50] L. S. I. Veiga, M. Etter, K. Glazyrin, F. Sun, C. A. Escanhoela, G. Fabbris, J. R. L. Mardegan, P. S. Malavi, Y. Deng, P. P. Stavropoulos, H.-Y. Kee, W. G. Yang, M. van Veenendaal, J. S. Schilling, T. Takayama, H. Takagi, and D. Haskel, *Phys. Rev. B* **96**, 140402(R) (2017).
- [51] T. Takayama, A. Krajewska, A. S. Gibbs, A. N. Yaresko, H. Ishii, H. Yamaoka, K. Ishii, N. Hiraoka, N. P. Funnell, C. L. Bull, and H. Takagi, *Phys. Rev. B* **99**, 125127 (2019).
- [52] L. S. I. Veiga, K. Glazyrin, G. Fabbris, C. D. Dashwood, J. G. Vale, H. Park, M. Etter, T. Irifune, S. Pascarelli, D. F. McMorrow, T. Takayama, H. Takagi, and D. Haskel, *Phys. Rev. B* **100**, 064104 (2019).
- [53] J. A. Mydosh, *Spin Glasses: An Experimental Introduction* (Taylor & Francis, Abingdon, 1993).
- [54] H. Liu and G. Khaliullin, *Phys. Rev. Lett.* **122**, 057203 (2019).
- [55] K. A. Modic, B. J. Ramshaw, A. Shekhter, and C. M. Varma, *Phys. Rev. B* **98**, 205110 (2018).
- [56] K. Riedl, Y. Li, S. M. Winter, and R. Valentí, *Phys. Rev. Lett.* **122**, 197202 (2019).
- [57] E. J. Bergholtz, A. M. Läuchli, and R. Moessner, *Phys. Rev. Lett.* **105**, 237202 (2010).
- [58] A. J. Willans, J. T. Chalker, and R. Moessner, *Phys. Rev. Lett.* **104**, 237203 (2010).
- [59] R. Hentrich, M. Roslova, A. Isaeva, T. Doert, W. Brenig, B. Büchner, and C. Hess, *Phys. Rev. B* **99**, 085136 (2019).
- [60] I. Kimchi, J. G. Analytis, and A. Vishwanath, *Phys. Rev. B* **90**, 205126 (2014).